American Mineralogist, Volume 80, pages 231–238, 1995

# Quartz-coesite transition revisited: Reversed experimental determination at 500–1200 °C and retrieved thermochemical properties

KUNAL BOSE,* JIBAMITRA GANGULY
Department of Geosciences, University of Arizona, Tucson, Arizona 85721, U.S.A.

## ABSTRACT

We have determined the quartz-coesite transition by reversed experiments in a piston-cylinder apparatus in the range 500–1200 °C. The difference between the sample pressure and apparent pressure was calibrated by (1) studying the friction decay in the hysteresis loop defined by the relationship between apparent ("nominal") pressure and piston position in the compression and decompression cycles, and (2) determining the melting temperature of LiCl by DTA in pressure cells similar to those used in the reversal experiments and comparing the results with those determined in the gas apparatus. The equilibrium transition boundary can be expressed as $P$ (kbar) = 21.945 (±0.1855) + 0.006901 (±0.0003)$T$ (K). It is subparallel to, but ~1.5 kbar higher than, the transition boundary determined by Bohlen and Boettcher (1982). We have also retrieved the entropy [39.56 ± 0.2 J/(mol·K)] and enthalpy of formation (−907.25 ± 0.007 kJ/mol) from elements of coesite at 1 bar, 298 K, from our phase-equilibrium data and selected thermochemical data from the literature. From the characteristics of the hysteresis loop we conclude that the often-used practice of maintaining a constant nominal pressure by repeated pressure adjustment during an experiment leads to variation of pressure on the sample.

## INTRODUCTION

Retrieval of thermochemical properties from phase-equilibrium data involving coesite depends critically on the location of the quartz ⇌ coesite transition in $P$-$T$ space (e.g., Fei et al., 1990; Berman, 1988; Akaogi and Navrotsky, 1984). In addition, the low $P$-$T$ slope, the fast reaction rates, and the simple chemistry make the quartz ⇌ coesite equilibrium a good candidate for a pressure calibration curve in high-pressure apparatus, as suggested by Mirwald and Massonne (1980) and by Bohlen and Boettcher (1982). It is, therefore, not surprising that the quartz ⇌ coesite transition has been a subject of intense experimental investigation since Coes (1953) first synthesized this high-pressure polymorph of $SiO_2$, with at least 19 studies in the past 35 yr, which have been reviewed by Bohlen and Boettcher (1982) and Mirwald and Massonne (1980). Bohlen and Boettcher (1982) discussed the problems with the earlier studies arising from choice of starting material and uncertainty of pressure calibration and undertook a careful reinvestigation of this equilibrium. They used well-characterized samples of quartz and coesite as starting material and obtained tight reversals (i.e., limits on the equilibrium phase transition defined by both growth and breakdown of phases at each temperature) from 350 to 1000 °C in a piston-cylinder apparatus, using a NaCl pressure cell. The frictional pressure loss was calibrated independently by determining the melting temperature of LiCl in a similar pressure cell.

During our experimental investigation of a related problem, namely the dehydration of talc to enstatite plus quartz and coesite (Bose and Ganguly, 1993), we obtained results that could not be reconciled with the calibration of Bohlen and Boettcher (1982), unless there had been significantly greater frictional pressure loss in our experimental setup than we had reason to expect. We, thus, undertook a reinvestigation of the quartz ⇌ coesite transition along with a detailed study of the friction characteristics of our pressure cell. Using our phase-equilibrium data and utilizing the existing thermochemical data for quartz, we have also retrieved new thermochemical data for coesite.

## EXPERIMENTAL METHODS

### Apparatus and pressure cell

All experiments were conducted in an end-loaded piston-cylinder apparatus using WC cores (13% Co binder) with either ½-in. (1.27-mm) or ¾-in. (1.90-mm) internal diameters and WC pistons (6% Co binder). Figure 1 represents a schematic illustration of the design of ½-in. pressure cells used in this work. The ¾-in. cells are similar to the ½-in. cells except for the difference in the radial dimensions of various parts. The outer bushing of the pressure cell was fabricated by pressing CsCl of 99% purity. As noted by Elphick et al. (1985), CsCl has a lower thermal conductivity than other commonly used bushing materials, such as NaCl, and thus helps to maintain a

* Present address: Department of Geological and Geophysical Sciences, Princeton University, Princeton, New Jersey 08544, U.S.A.

0003–004X/95/0304–0231$02.00

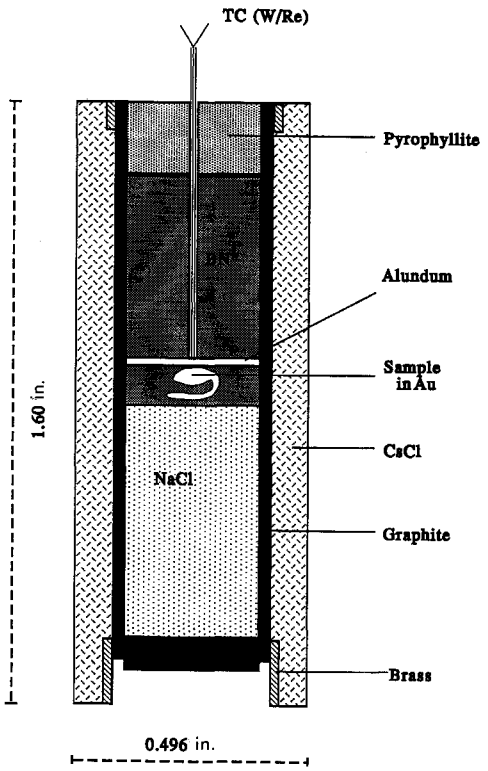


Fig. 1. Schematic of pressure cell used in the piston-cylinder apparatus.

relatively lower temperature at the carbide core, thereby minimizing its mechanical failure or cracking. The pressure cell was wrapped with Pb foil 0.025 mm thick and painted on the outside with H-free $MoS_2$ lubricant (Molykote G-n paste from Dow Corning Ltd.) to reduce friction between the pressure cell and the carbide core. $MoS_2$ grease was also applied to the outer surface of the piston to minimize friction between the carbide core and the piston.

### Measurement of nominal pressure and temperature

Since friction characteristics of the experimental assembly in a piston-cylinder apparatus depend on whether the piston is in an intrusion (piston-in) or an extrusion (piston-out) mode when the desired nominal pressure is achieved, we have carefully monitored the piston displacement throughout an experiment by a linear differential transducer, which was linked to the piston, and had a resolution of $10^{-5}$ in. The piston was always in an intrusion mode when the cell was compacted to a desired nominal pressure. The pressure cell was pressurized very slowly (~0.05 kbar/min) at room temperature, to approximately 10–20% lower than the desired experiment pressure, and left overnight. This was done to ensure thorough compaction of the cell material and mechanical stability of the thermocouple. Heating of the cell to the desired temperature caused the nominal pressure to increase (~3–7%, depending on temperature) because of the thermal expansion of the cell, with concomitant extrusion of the piston. After reaching a temperature 10–15 °C lower than the desired temperature, the cell was brought up to the final nominal pressure, followed by ramping to the final temperature.

Pressure was monitored by a Heise gauge 16 in. in diameter, calibrated to the NBS standard immediately prior to the current set of experiments, and also by an on-line digital pressure transducer. The analogue signals from the pressure and displacement transducers and the thermocouple were monitored by a 22-bit A/D converter (Analog Devices AD1170). The temperature set points were set through 14-bit D/A converters (Intersil ICL7134). An IBM personal computer was interfaced with the converters for setting, monitoring, and logging all parameters. The thermocouple signal was preamplified by a 100× instrumentation amplifier (maximum gain error 0.02%) and the thermocouple cold junction was corrected with a cold-junction correction integrated circuit (maximum error 0.5 °C). The emf of the thermocouple was also measured before the preamplifier and cold junction correction by a calibrated digital voltmeter with a resolution of 0.01 mV.

### Starting material and reversal procedure

An $\alpha$-quartz sample was prepared by firing puratronic-grade $SiO_2$ (Johnson Matthey) at 800 °C for 48 h. X-ray diffraction of the product, as well as oil-immersion optical microscopy, showed it to be pure $\alpha$ quartz. Coesite was synthesized from this quartz at 700 °C, 31–32 kbar, for 70 h, in sealed Au capsules. X-ray diffraction and oil immersion microscopy showed the product to be pure coesite with grain sizes of 10–20 $\mu$m.

For reversal experiments, approximately equal amounts of quartz and coesite were mixed together in a SPEX mixer for about 1 min. Relative peak heights of the phases in X-ray diffraction of different portions of the starting mixture showed that the mixture was essentially homogeneous. Around 5–10 mg of this mixture was loaded into 2.38-mm Au capsules, moistened with water, and sealed under a carbon arc. The capsule was folded with the sample on one side of the fold and placed inside the pressure cell such that the sample segment coincided with the central section of the furnace. A thin (0.254 mm) aluminum oxide disk was placed above the capsule to prevent it from being punctured by the rigid thermocouple ceramic during compression of the cell. At the end of the experiment, the temperature was quenched to the ambient condition within 15–20 s. The Au capsule after each experiment showed an indentation mark of the thermocouple tip, ensuring that the thermocouple junction recorded the sample temperature. As discussed below, there was a progressive decay of friction with time, leading to an effectively frictionless condition in about 30 h or less at the conditions of our experiments. Thus all reversal experiments were designed to last between 50 and 100 h

so that the final nominal pressure effectively represented the true sample pressure.

The experimental products were analyzed by X-ray diffraction and optical microscopy. Comparison of the relative intensities of (100) and (101) peaks for $\alpha$ quartz and (111) and (002) peaks of coesite from diffractograms before and after each experiment allowed unequivocal determination of the direction of reaction.

## Pressure calibration in the piston-cylinder apparatus

In a piston-cylinder apparatus, the experimental sample is subjected to a pressure (referred here as sample pressure) which may be greater, equal to, or less than the nominal pressure, which is the pressure calculated by dividing the applied force by the cross-sectional area of the piston used to compress the pressure cell. The extent of departure of the sample pressure from the nominal pressure, which is referred as net friction, depends on a number of factors, viz. (1) the mode of piston movement (piston-in or piston-out) to the desired nominal pressure, (2) the nature of pressure cell, and (3) the $P$-$T$ conditions and duration of an experiment.

We have carried out a detailed study of the characteristics of hysteresis loops defined by the relationship of nominal pressure vs. piston position in both piston-in and piston-out modes. This analysis permitted an estimate of the friction in our pressure cell as a function of time. In addition, we have also determined the melting temperature of LiCl as a function of pressure and time. Comparison of these data with the melting curve determined by Clark (1959) in a gas apparatus permitted further evaluation of friction in our experimental assembly. Of all the salts studied by Clark, the melting curve of LiCl is closest to the $P$-$T$ boundary between quartz and coesite, and therefore would most closely reflect the friction characteristics of our pressure cell near the quartz-coesite transition.

### Hysteresis studies

Since the shear strength of the salts decreases with increasing temperature, the extent of friction correction should change with temperature. We have, thus, conducted hysteresis studies at 500 and 800 °C with pressure cells with both ½-in. and ¾-in. o.d., which were similar to the ones used in the determination of the quartz-coesite transition. Figure 2 shows the hysteresis loop for a ½-in. cell at 500 °C. After initial pressurization to 28.8 kbar and heating to 500 °C (point A), the pressure was increased again to 35.6 kbar (point C). A pressure increase of around 3 kbar (A to B) was required before the piston started intruding again. The pressurizing pump and the valve to the ram driving the piston (master ram) were turned off at 35.6 kbar (point C). The piston, however, continued to intrude with a corresponding decrease in nominal pressure (C to D) as a result of the decay of friction with time. By the time the piston reached point D, enough heat was conducted to the hydraulic oil in the piston ram to cause it to expand sufficiently, thus leading to an increase of nominal pressure from D to E, which corresponds to a pressure increase of ~200 bars. Following a suggestion of I. C. Getting (personal communication), we virtually eliminated this problem of pressure increase due to the heating of the hydraulic oil in subsequent experiments by preheating and maintaining the hydraulic oil in the piston ram at a constant temperature of 60 °C. From E to F, the friction continued to decay over a period of 24 h, as indicated by the fall in nominal pressure and the simultaneous intrusion of the piston. The total decay in nominal pressure over this 24 h period is ~3.5%. At this stage, the nominal pressure was increased by turning on the hydraulic pump. When the nominal pressure reached 40.3 kbar (G), the pump was stopped, the inlet pressure valves were closed, and the bleed valves were opened to commence the decompression cycle. However, even with the pressure in the line decreasing, the piston continued to intrude (G to X), indicating that the true pressure was still lower than the nominal pressure. The piston stopped intruding at point X and began to extrude at point Z on the hysteresis loop.

Since the piston-in mode implies that $P$ (nominal) > $P$ (sample) or positive net friction, whereas the piston-out mode implies the reverse condition, the state on the hysteresis loop separating the piston-in and piston-out modes should represent essentially a state of zero net friction (ZNF). Thus, the ZNF state should lie between points X and Z on the hysteresis loop. A similar exercise of reaching a desired nominal pressure, as in the upstroke part of the cycle, that is, closing the valves to the master ram, waiting, and then going to a new nominal pressure, was repeated during the downstroke.

On the second compression cycle (starting at L), the decay of friction with time was considerably smaller because of the well-compacted state of the pressure cell. There was no further decay of friction beyond the point N, which was reached ~12 h after shutting off the pressurizing pump and the valve to the master ram at point M on the hysteresis loop. (This property of the second compression cycle was noticed earlier by Mirwald et al., 1975, in their detailed study of friction characteristics of pressure cells by DTA experiments in a piston-cylinder apparatus). We thus conclude that point N represents essentially a zero net friction (ZNF) condition within the hysteresis loop. A line drawn through N parallel to the nearly constant slope of the compression cycle of the hysteresis loop above 34 kbar should then define the locus of ZNF conditions. It is interesting to note that this line passes between points X and Z, which, as deduced above, must lie on two sides of the ZNF friction line within the hysteresis loop. The time needed to attain this frictionless condition from a point in the hysteresis loop in the first compression cycle should essentially equal the time from E to F plus M to N, which amounts to 36.13 h. Additional experiments at 500 °C with a ¾-in. cell and at 800 °C with both ½-in. and ¾-in. cells show that higher tem-

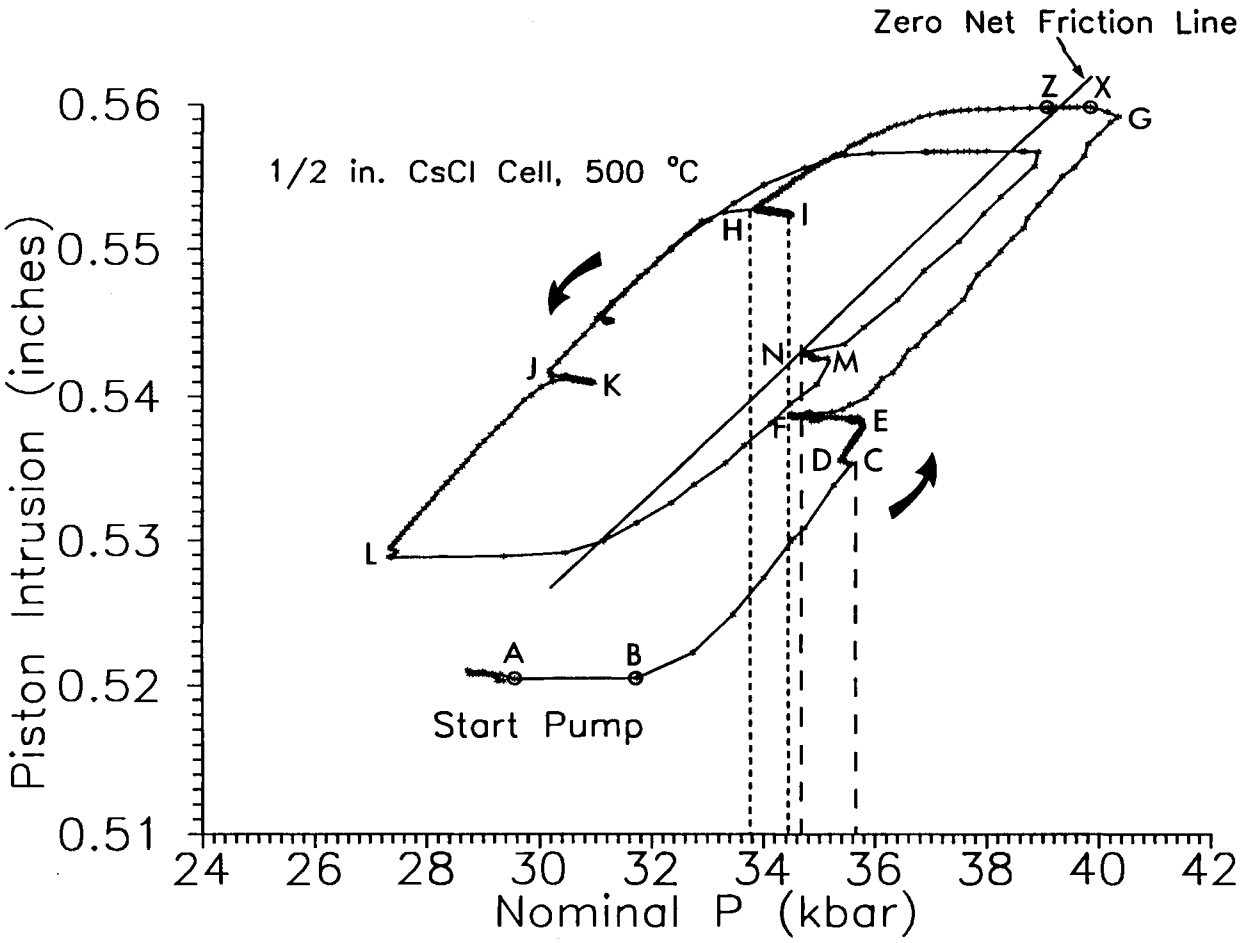


Fig. 2. Piston displacement vs. nominal pressure (hysteresis loop) of a ½-in. pressure cell (Fig. 1) in the piston-cylinder apparatus at 500 °C. The outer and inner loops represent first and second compression-decompression cycles, respectively.

peratures cause a faster decay of friction, which is expected because of the softening of the cell, whereas a larger diameter does not seem to have any significant effect on the decay characteristics, at least within the range of the investigated conditions.

It should be noted that the often-used practice of maintaining a fixed nominal pressure during an experiment by repeated pumping and bleeding of hydraulic fluid essentially causes a variation of true pressure. This point can be easily appreciated by considering points C and E on the hysteresis loop, which are essentially at the same nominal pressure. The true pressures corresponding to these positions are given by the projections of the decay paths C-D and E-F on to the ZNF line within the hysteresis loop. A better approach to maintaining a nearly constant sample pressure is to leave the system alone after pumping (piston-in mode) and shutting off the valves, provided that there is no leak in the system. In this case the nominal pressure will progressively decay toward true pressure. The latter may slightly increase because of the compaction of the cell during this process, even if the nominal pressure has decreased, and will be less than or equal to the last recorded nominal pressure.

The asymmetric nature of the hysteresis loop with respect to the ZNF line is incompatible with the assumption made in several earlier studies (Akella, 1979) that the true pressure lies halfway between the compression and decompression envelopes. It seems to us that the primary reason for this asymmetry of the hysteresis loop lies in the difference between the rates of compression and decompression of the pressure cell. Typically, a pressure cell is compressed at much slower rate than it is decompressed. The mechanics of the bleed valve limits the decompression rate. For instance, it took about 2.25 h to increase nominal pressure by 6 kbar (F to G), whereas the same extent of decompression was accomplished in only 55 min (G to H). It is our experience that friction (whether positive or negative) is larger when the rate of nominal pressure change is faster. The above findings about the asymmetry of the hysteresis loop are consistent

with the observations of Mirwald et al. (1975), and Mirwald and Massonne (1980).

### DTA study of melting of LiCl

The melting temperatures of LiCl and of several other alkali halides were determined by Clark (1959) up to 25 kbar in a gas apparatus. Subsequent studies by Morse (1970) and Bohlen and Boettcher (1982) of the melting temperatures of alkali halides in a gas apparatus indicate that Clark's data are systematically 10–15 °C too low, possibly because of the presence of absorbed moisture in the highly hygroscopic salts, a potential problem also noted by Clark. (Morse, 1970, determined the melting temperature by DTA, whereas Bohlen and Boettcher, 1982, determined the melting temperature by noticing the onset of drop of Pt spheres in the alkali halides.) We have thus added 10 °C to the melting temperatures determined by Clark (1959) for LiCl. To facilitate comparison with published literature values, no pressure correction was applied to the thermocouple emf.

The procedure for DTA study used in this work was similar to that developed and refined in the laboratory of George C. Kennedy in the 1960s and 1970s (e.g., Akella and Kennedy, 1971; Mirwald et al., 1975). The sample container was machined from ultrapure Fe rods from Sigma Chemicals. Ultrapure (99.995%) and ultradry LiCl from AESAR was packed into a sample container and a 0.005-in. oversized lid was fitted to the container by pressing. A 0.001-in. undersized sleeve of Fe was then slipped on over the capsule to prevent molten LiCl from leaking out during the experiment and poisoning the thermocouple. To prevent absorption of moisture, the entire process of opening the bottle of LiCl, packing the salt into the sample container, and fitting the lid was carried out in a desiccator glove box filled with dry $N_2$ gas, and the assembly was immediately transferred into a vacuum drying oven maintained at 150 °C. Thermocouple wires of Pt and 10% Rh/Pt, manufactured, calibrated, and certified by Engelhard Corporation were sheathed in 4-hole, high-purity (99.9%) alumina tubes 1.6 mm in diameter. The reference junction was situated in a notch ground into the side of the tube, ~3 mm above the tip. Both the reference and sample junctions were covered with high-purity alundum cement and fired in air to a red-hot temperature (~900 °C).

The DTA signals associated with the melting of CsCl were very sharp and enabled unambiguous determination of the melting temperatures. A typical DTA signal from one of our experiments is shown in Figure 3. Melting temperatures and pressures were read just at the onset of melting and automatically recorded in the computer. The software specially written for DTA experiments recorded the nominal pressure during the DTA scan. In order to obtain sharp DTA signals, the temperature was raised rapidly at a rate of ~20 °C/s, as is the usual practice, near the melting temperature. This caused a pressure increase of ~100–150 bars. The melting temperature at a fixed nominal pressure was averaged from three to five scans,

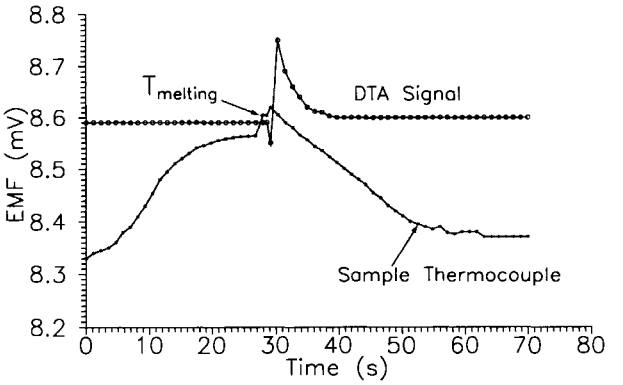


Fig. 3. Representative DTA signal due to melting of LiCl at a nominal pressure of 16 kbar, using ½-in. salt pressure cell (Fig. 1). Dots represent time of recording data in a computer.

generally reproducing to within 0.005 mV (equivalent to <1 °C) for Pt-Rh thermocouples.

The results of the determination of the melting temperature of LiCl between 10 and 25 kbar are illustrated in Figure 4A. Subsequent scans were repeated at desired time intervals at essentially a fixed nominal pressure to analyze the decay of friction with time for our ½-in. and ¾-in. pressure cells. The results are illustrated in Figure 4B in terms of percent deviation from true pressure, $\Delta P\%$, vs. time, where $\Delta P$ equals the difference between the nominal pressure at a melting temperature, $T$, as determined by DTA, and the pressure at $T$ given by the melting curve of LiCl determined by Clark (1959) (and corrected as discussed above). We found from the DTA studies that the initial friction was 6.5% of nominal pressure for the ½-in. cell and 4.5% of nominal pressure for the ¾-in. cell and that the friction decayed completely within 30 h for both cells. These results are consistent with those derived from hysteresis studies. Thus, we can confidently accept the recorded gauge pressure at the end of each experiment of longer than 40-h duration as representing the true pressure on the sample. Consequently, we carried out all reversal experiments in the true piston-in mode with experiment durations of 50–100 h and accepted the final nominal pressure as the true sample pressure.

## Experimental results

The results of our reversal experiments on the quartz-coesite transition are summarized in Table 1, and illustrated in Figure 5. The reversal data yield a tightly constrained linear phase boundary over the temperature range 500–1100 °C, which can be expressed as

$$P\,(\text{kbar}) = 21.945\ (\pm 0.1855) + 0.006901\ (\pm 0.0003)T\,(\text{K}). \quad (1)$$

Also shown for comparison are the results obtained by Bohlen and Boettcher (1982) and Mirwald and Massonne (1980). The reaction boundary determined in this study

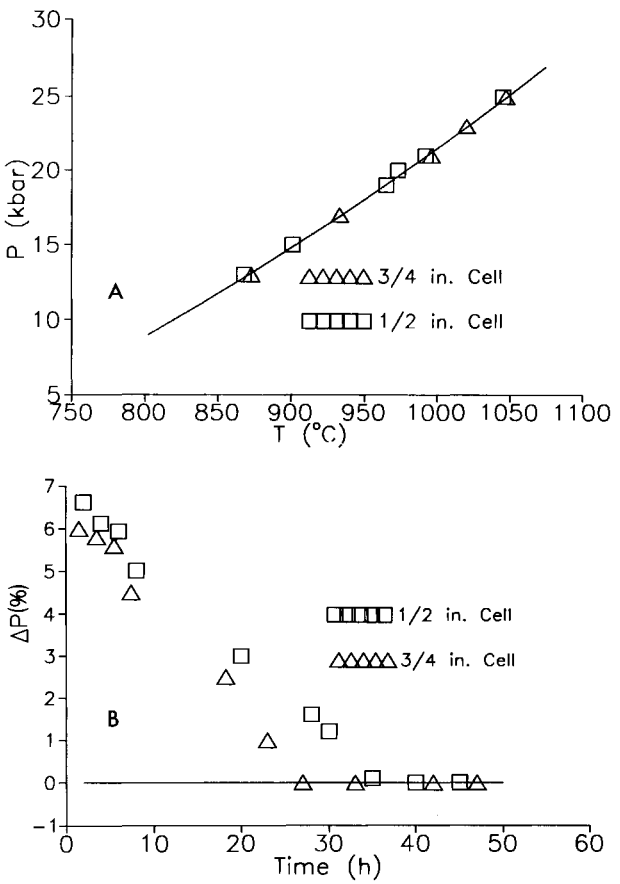


Fig. 4. (**A**) Melting temperature of LiCl as a function of nominal pressure, as determined by DTA experiments, 34 h after initial pressurization of pressure cell. Squares represent melting temperatures determined in ½-in. salt cells (Fig. 1), whereas the triangles correspond to those determined in ¾-in. salt cells, which are similar to the ½-in. salt cells, except for the dimensions of the various parts. The solid line is the melting curve of LiCl as determined by Clark (1959) in a gas apparatus, including a +10 °C correction, as suggested by Morse (1970) and Bohlen and Boettcher (1982). (**B**) Illustration of the decay of friction with time in ½-in. and ¾-in. salt cells (Fig. 1 and its scaled-up version), as determined by the drift in the emf corresponding to the DTA signal for melting of LiCl as a function of time. The $\Delta P\%$ represents the percentage deviation of the nominal pressure from the true pressure at the melting temperature recorded by DTA.

has essentially the same slope as, but is ~1.5 kbar higher than, that determined by Bohlen and Boettcher (1982). We are unable to sort out the reason for this discrepancy of pressure. Bohlen and Boettcher have calibrated the friction in their 1-in. NaCl cell by determining the melting points of several alkali halides using the sinking Pt-sphere method. Their results agreed with the corrected melting curve of Clark (1959), indicating that their 1-in. NaCl cell had no friction as well. To explain the discrepancy between the two sets of data, we considered the possibility that the process of grinding the starting material in an agate mortar, as was done by Bohlen and

**Table 1.** Experimental conditions and results for quartz ⇌ coesite transition

| Expt. | $T$ (°C) | $P$ (kbar) | $t$ (h) | Result |
|---|---|---|---|---|
| QC39 | 500 | 27.1 | 71 | 100% quartz |
| QC38 | 500 | 27.4 | 67.5 | 100% coesite |
| QC37 | 600 | 28.2 | 56 | 99% coesite |
| QC36 | 600 | 27.8 | 60 | 95% quartz |
| QC10 | 700 | 28.5 | 72 | 100% quartz |
| QC12 | 700 | 28.8 | 70 | 90% coesite |
| QC27 | 800 | 29.6 | 57 | 100% coesite |
| QC30 | 800 | 29.2 | 50 | 100% quartz |
| QC22 | 900 | 29.8 | 48 | 100% quartz |
| QC21 | 900 | 30.1 | 48 | 95% coesite |
| QC23 | 1000 | 30.6 | 47 | 100% quartz |
| QC25 | 1000 | 30.9 | 48 | 100% coesite |
| QC1 | 1100 | 31.1 | 36 | 100% quartz |
| QC9 | 1100 | 31.5 | 36 | 100% coesite |
| QC28 | 1200 | 32.0 | 32 | 100% quartz |
| QC33 | 1200 | 32.4 | 30 | 100% coesite |

Boettcher, could have preferentially introduced more strain energy to quartz, thereby increasing the field of stability of coesite with respect to quartz. However, some of our reversals were conducted with two capsules placed next to each other in the pressure cell, one containing starting material that was ground in an agate mortar and the other containing unground starting material. Both showed the same change in reaction direction after the experiment. Experiments were then carried out using our starting material and that used by Bohlen and Boettcher in their reversal experiments (the starting material was kindly provided by Steve Bohlen). Once again, no differences in reaction direction were found, except that the experimental products using the Bohlen and Boettcher starting material were much smaller in grain size than ours.

## Thermochemical analysis

Akaogi and Navrotsky (1984) have calculated the quartz-coesite transition boundary on the basis of measured and derived thermochemical data, which were constrained by the experimental data of Bohlen and Boettcher (1982). Their calculated transition is in good agreement with the reversed experimental data of Bohlen and Boettcher but has a significant curvature outside of the range of the experimental data. The reason for the curvature of the calculated phase boundary lies in their use of $C_P$ data of coesite from Watanabe (1982), which have a thermodynamically unacceptable form in that the $C_P$ increases at nearly constant rate above 200 °C. Subsequent evaluations (e.g., Berman, 1988; Holland and Powell, 1990; Fei et al., 1990) have preferred the $C_P$ data for coesite and quartz in the thermochemical tabulation of Robie et al. (1978) and Hemingway (1987), respectively. As discussed below, we have retrieved the enthalpy of formation and entropy of coesite from our experimental data on the quartz-coesite transition, using the $C_P$ (coesite) data from Robie et al. (1978) and other commonly accepted thermochemical and volumetric properties for quartz and coesite, as required in the calculation. At any

condition along an equilibrium boundary, we have

$$\Delta G(P,T) = 0$$

$$= \Delta H(1,T) - T\Delta S(1,T) + \int_1^P \Delta V \, dP \quad (2)$$

or

$$\Delta H(1,298) - T\Delta S(1,298) + \left[\int_{298}^T \Delta C_P \, dT - T\int_{298}^T \frac{\Delta C_P}{T} dT + \int_1^P \Delta V \, dP\right] = 0 \quad (3)$$

where $G$, $H$, $S$, and $V$ stand for Gibbs free energy, enthalpy, entropy, and volume, respectively. For brevity, a property of a pure phase at 1 bar, 298 K, will henceforth be referred to as a reference state property and designated by the symbol $Y^0_{298}$, where $Y$ is the property of interest. Explicit evaluation of the terms within the brackets of Equation 3 yields $\phi = \Delta H^0_{298} - T\Delta S^0_{298}$ for a set of temperatures. Linear regression of $\phi$ vs. $T$ then yields $\Delta H^0_{298}$ and $\Delta S^0_{298}$ as the intercept and slope terms, respectively. We have followed the above procedure to retrieve $\Delta H^0_{298}$ and $\Delta S^0_{298}$ for the quartz-coesite transition from our experimental data, which were then combined with the $\Delta H^0_f$ and $S^0$ values of quartz at 1 bar, 298 K (Berman, 1988), to determine the corresponding thermochemical properties of coesite.

The molar volumes of the phases were expressed as a function of $P$ and $T$ according to the thermodynamic relation

$$V(P,T) = V^0_{298}\left(1 + \int_{298}^T \alpha \, dT - \int_1^P \beta \, dP\right) \quad (4)$$

where $\alpha$ is the isobaric thermal expansivity and $\beta$ is the isothermal compressibility, it being assumed that $\beta$ is independent of temperature. It was assumed that within the $P$-$T$ range of interest, $\alpha$ and $\beta$ vary linearly with temperature and pressure, respectively, according to $\alpha = \alpha_0 + \alpha_1 T$, and $\beta = \beta_0 + \beta_1 P$. The constants $\alpha_0$, $\alpha_1$, $\beta_0$, and $\beta_1$ were determined by least-square regression of the volume expansion (Skinner, 1966) and compression (McSkimin et al., 1965, for quartz; Levien and Prewitt, 1981, for coesite) data.

The reference state enthalpy, entropy, and molar volume of $\alpha$ quartz, as listed in Hemingway (1987), have been used in the currently available optimized thermochemical data bases (e.g., Berman, 1988; Holland and Powell, 1990) and are thus accepted in the present calculations. The expressions for heat capacity and molar volume of quartz as functions of temperature are complicated by the $\alpha$-$\beta$ transition occurring at 848 K, 1 bar. We have used the $C_P$ expression of quartz from Berman and Brown (1985) and Berman (1988), who expressed the $C_P$ over the $\lambda$ transition range as a sum of lattice and $\lambda$ components. The lattice component represents a smooth extension of the $C_P$ of $\alpha$ quartz. From reviewing the available $C_P$ data for quartz, Berman and Brown (1985) computed the $\lambda$ component of $C_P$ between 373 and 848 K, 1 bar, allowing reasonable fit to the calorimetric data to within 30 K of the $\lambda$ point. The lattice component of both $\alpha$ and $\beta$ quartz was represented by the same parameterized function. Since $C_P$ data are lacking as a function of pressure, Berman and Brown (1985) assumed that the magnitude of $C_{P\lambda}$ and the width of the transition is independent of pressure. Changes in $H$ and $S$ due to the $\lambda$ transition were computed by performing the appropriate integrations of the $C_{P\lambda}$ expression to obtain the change in free energy resulting from this transition. The effect of the transition on the volume was calculated by taking the pressure derivative of $G_\lambda$.

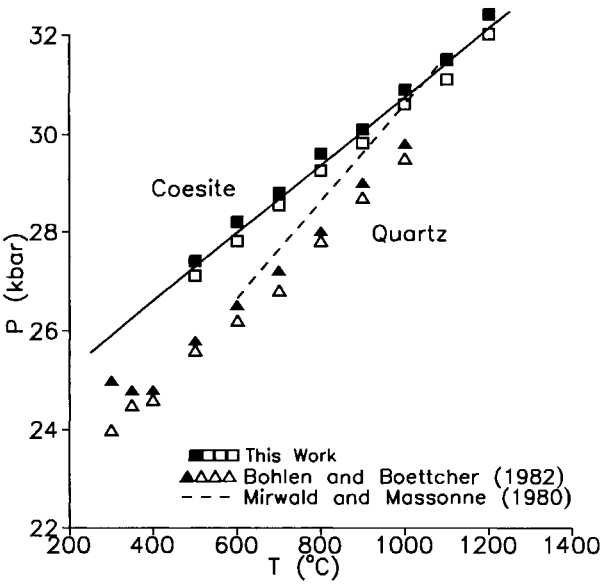


Fig. 5. Comparison of the $\alpha$-quartz = coesite transition as experimentally determined in this work (squares), by Bohlen and Boettcher, 1982 (triangles), and by Mirwald and Massonne, 1980 (dashed line). Open symbols: growth of quartz at the expense of coesite; solid symbols: the reverse process. The solid line: the equilibrium boundary of the $\alpha$-quartz = coesite transition using the enthalpy and entropy of coesite as retrieved from phase-equilibrium data of the present study.

We have solved Equation 3 to obtain $\phi$ ($T$) using the best fit line through the reversal brackets (Eq. 1) as the equilibrium phase boundary. Regression of $\phi$ vs. $T$ and combination of the retrieved $\Delta H^0_{298}$ and $\Delta S^0_{298}$ with the $\Delta H^0_f$, and $S^0$ for quartz (Berman, 1988) yields enthalpy of formation from elements $H^0_{f,298}$ of $-907252.3$ ($\pm 7.2$) J/mol and $S^0_{298} = 39.558$ J/(mol·K) for coesite. Instead of using Equation 1, we have also used the conditions on the reversal brackets as equilibrium conditions. Each reversal bracket was expanded to take into account the uncertainty of temperature ($\pm 5$ °C) and pressure ($\pm 200$) measurements. This approach yields the solution for Equation 3, and regression of the $\phi$ values vs. $T$ yields $H^0_{f,298} = -907225.6$ ($\pm 27.48$) J/mol and $S^0_{298} = 39.5815$ ($\pm 0.046$) J/(mol·K) for coesite, which are essentially the same as derived above. These retrieved thermochemical

**TABLE 2.** Summary of standard-state enthalpy of formation from elements and the third law entropy of coesite from existing literature data and that retrieved from phase-equilibrium data on the quartz = coesite transition (this work)

| | | RHF '78 | B88 | A&N '84 | This work |
|---|---|---|---|---|---|
| Coesite | $H^0_{298}$ kJ/mol | −905.6 ± 2.1 | −907.6 | −907.7 | −907.25 ± 0.007 |
| | $S^0_{298}$ J/(mol·K) | 40.38 ± 0.42 | 39.424 | 38.53 | 39.56 ± 0.02 |
| Coes-Qtz* | $H^0_{298}$ kJ/mol | −5.116 | −3.096 | −2.93 ± 0.3 | −3.45 |
| | $S^0_{298}$ J/(mol·K) | −1.0877 | −2.03 | −2.93 | −1.9 |

*Note:* RHF '78 = Robie et al. (1978); B88 = Berman (1988); A&N '84 = Akaogi and Navrotsky (1984).
* $H^0_{298}$ and $S^0_{298}$ for $\alpha$ quartz are from Hemingway (1987).

properties of coesite are compared with existing literature values in Table 2. Our enthalpy value agrees very well with that determined by Akaogi and Navrotsky (1984) from calorimetric measurements and also with that listed by Berman (1988) in his internally consistent data base. Our $S^0_{298}$ value for coesite is within the range of the data available in the literature and closest to the value derived by Berman [$S^0_{298}$ = 39.424 J/(mol·K)]. Figure 5 shows the quartz-coesite transition boundary (solid line) calculated from the thermochemical data of coesite, as retrieved above, and those of quartz derived by Berman (1988).

## ACKNOWLEDGMENTS

This research was partly supported by a NASA grant no. NAGW 1332. We are thankful to Steve Bohlen for providing us with the starting mixture of quartz and coesite used in experimental study reported in Bohlen and Boettcher (1982). The paper has benefited from the careful reviews of Steve Bohlen and Ivan Getting.

## REFERENCES CITED

Akaogi, M., and Navrotsky, A. (1984) The quartz-coesite-stishovite transformations: New calorimetric measurements and calculation of phase diagrams. Physics of the Earth and Planetary Interiors, 36, 124–134.

Akella, J. (1979) Quartz-coesite transition and the comparative friction measurements in the piston-cylinder apparatus using talc-alsimag-glass (TAG) and NaCl high-pressure cells. Neues Jahrbuch für Mineralogie Monatshefte, H5, 217–224.

Akella, J., and Kennedy, G.C. (1971) Melting of gold, silver, and copper: Proposal for a new high pressure calibration scale. Journal of Geophysical Research, 76, 4969–4977.

Berman, R.G. (1988) Internally-consistent thermodynamic data for minerals in the system $Na_2O$-$K_2O$-CaO-MgO-FeO-$Al_2O_3$-$SiO_2$-$TiO_2$-$H_2O$-$CO_2$. Journal of Petrology, 29, 445–522.

Berman, R.G., and Brown, T.H. (1985) The heat capacity of minerals in the system $Na_2O$-$K_2O$-CaO-MgO-FeO-$Al_2O_3$-$SiO_2$-$TiO_2$-$H_2O$-$CO_2$: Representation, estimation, and high temperature extrapolation. Contributions to Mineralogy and Petrology, 89, 168–183.

Bohlen, S.R., and Boettcher, A.L. (1982) The quartz = coesite transformation: A precise determination and the effects of other components. Journal of Geophysical Research, 87(88), 7073–7078.

Bose, K., and Ganguly, J. (1993) Stability of talc at high pressures: Experimental determination, retrieval of thermodynamic properties, and applications to subduction processes. Geological Society of America Abstracts with Programs, 25, 213–214.

Clark, S.P. (1959) Effect of pressure on the melting point of eight alkali halides. Journal of Chemical Physics, 31, 1526–1531.

Coes, L., Jr. (1953) A new dense crystalline silica. Science, 118, 131–132.

Elphick, S.C., Ganguly, J., and Loomis, T.P. (1985) Experimental determination of cation diffusivities in aluminosilicate garnets: I. Experimental methods and interdiffusion data. Contributions to Mineralogy and Petrology, 90, 36–44.

Fei, Y., Saxena, S.K., and Navrotsky, A. (1990) Internally consistent thermodynamic data and equilibrium phase relations for compounds in the system MgO-$SiO_2$ at high pressure. Journal of Geophysical Research, 95(B5), 6915–6928.

Hemingway, B.S. (1987) Quartz: Heat capacities from 340 to 1000 K and revised values for the thermodynamic properties. American Mineralogist, 72, 273–279.

Holland, T.J.B., and Powell, R. (1990) An enlarged and updated internally consistent thermodynamic dataset with uncertainties and correlations: The system $K_2O$-$Na_2O$-CaO-MgO-FeO-$Fe_2O_3$-$Al_2O_3$-$TiO_2$-$SiO_2$-C-$H_2$-$O_2$. Journal of Metamorphic Geology, 8, 89–124.

Levien, L., and Prewitt, C.T. (1981) High-pressure crystal structure and compressibility of coesite. American Mineralogist, 66, 324–333.

McSkimin, H.J., Andreatch, P., Jr., and Thurston, R.N. (1965) Elastic moduli of quartz versus hydrostatic pressure at 25°C and −195.8°C. Journal of Applied Physics, 36, 1624–1632.

Mirwald, P.W., and Massonne, H.-J. (1980) The low-high quartz and quartz coesite transition to 40 kbar between 600°C and 1600°C and some reconnaissance data on the effect of $NaAlO_2$ component on the low quartz-coesite transition. Journal of Geophysical Research, 85, 6983–6990.

Mirwald, P.W., Getting, I.C., and Kennedy, G.C. (1975) Low-friction cell for the piston cylinder high pressure apparatus. Journal of Geophysical Research, 80, 1519–1525.

Morse, S.A. (1970) Alkali feldspars with water at 5 kb. Journal of Petrology, 11, 221–251.

Robie, R.A., Hemingway, B.S., and Fisher, J.R. (1978) Thermodynamic properties of minerals and related substances at 298.15 K and 1 bar ($10^5$ Pascals) pressure and at higher temperatures. U.S. Geological Survey Bulletin, 1452, 456 p.

Skinner, B.J. (1966) Thermal expansion. In S.P. Clark, Ed., Handbook of physical constants. Geological Society of America Memoir, 97, 75–96.

Watanabe, H. (1982) Thermochemical properties of synthetic high-pressure compounds relevant to the Earth's mantle. In S. Akimoto and M.H. Manghnani, Eds., High-pressure research in geophysics, p. 441–464. Center for Academic Publications, Tokyo.

MANUSCRIPT RECEIVED MAY 9, 1994
MANUSCRIPT ACCEPTED NOVEMBER 21, 1994